Supporting Information

Unveiling the Role of Electrode Architecture and Illumination Direction in Heterojunction Photo-Supercapacitors Performance and Charge Storage Mechanism

Zohreh Hosseini [a], *Mohamad Mohsen Momeni* [a]*, *A. Wouter Maijenburg* [c,d], *Fuxiang Zhang* [c]

[a] *Department of Chemistry, Isfahan University of Technology, Isfahan 84156-83111, Iran, *mm.momeni@cc.iut.ac.ir*

[b] *Inorganic Chemistry, Institute of Chemistry, Martin-Luther-University Halle-Wittenberg, Kurt-Mothes-Straße 2, 06120 Halle (Saale), Germany*

[c] *Center for Innovation Competence SiLi-Nano, Martin-Luther-University Halle-Wittenberg, Karl-Freiherr-von-Fritsch-Straße 3, 06120 Halle (Saale), Germany*

[d] *State Key Laboratory of Catalysis, Dalian Institute of Chemical Physics, Chinese Academy of Sciences, Dalian National Laboratory for Clean Energy. 116023 Dalian, P R China*

1. Characterization

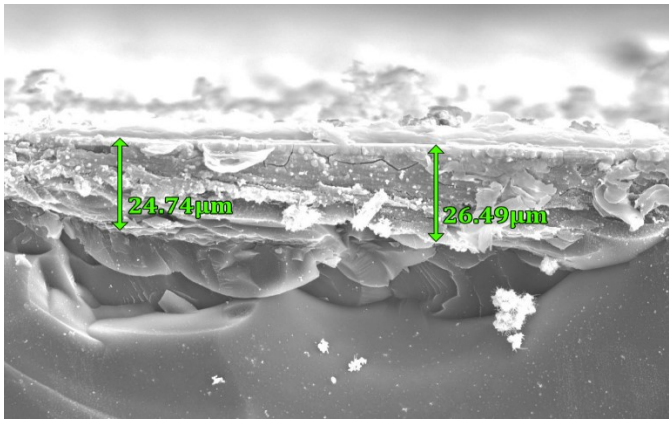

Fig. S1 Cross-section image of the BVO electrode shows the thickness of this film on FTO.

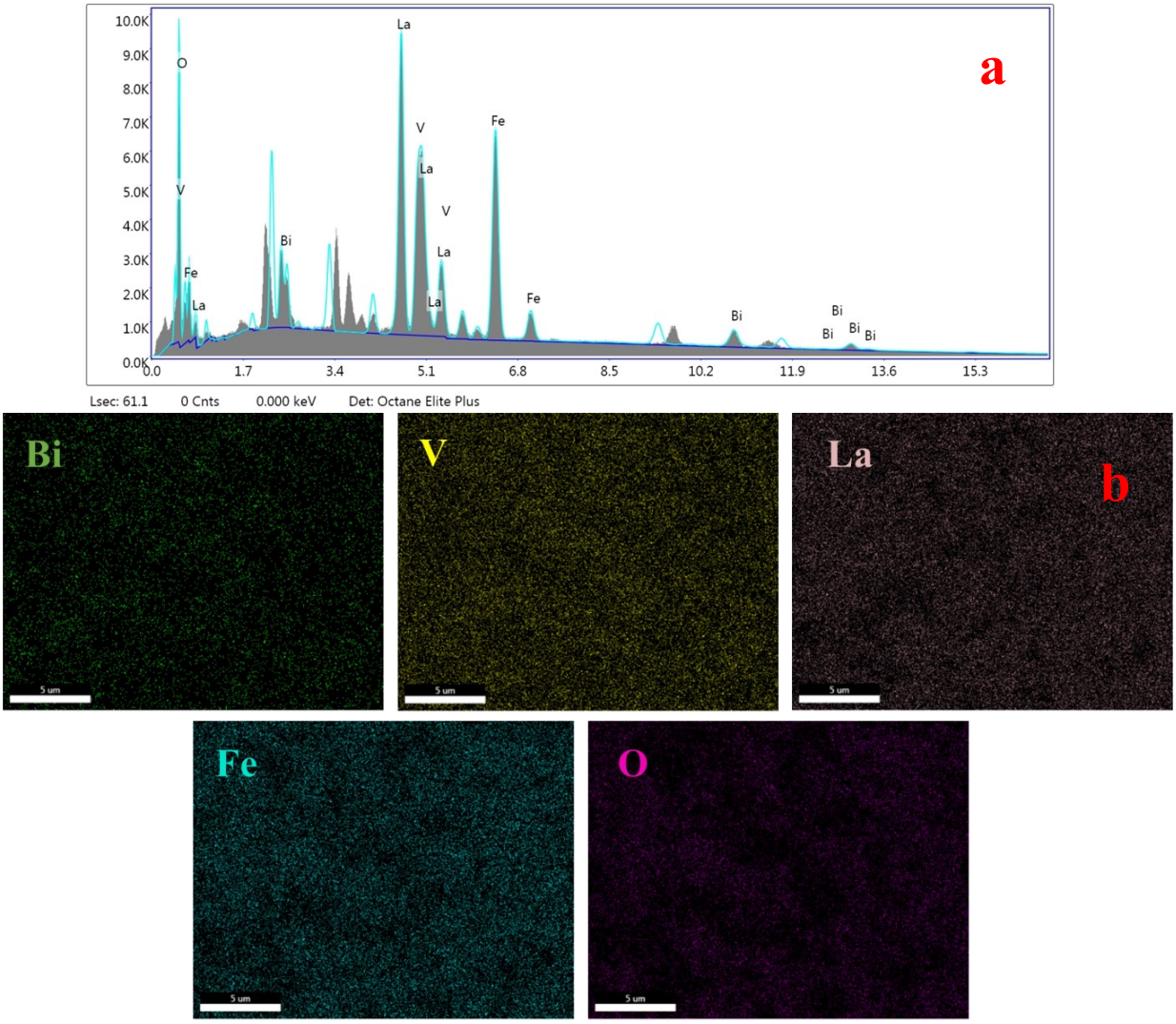

Fig. S2 (a) EDS spectrum and (b) EDS-mapping of sample 12-LFO@BVO.

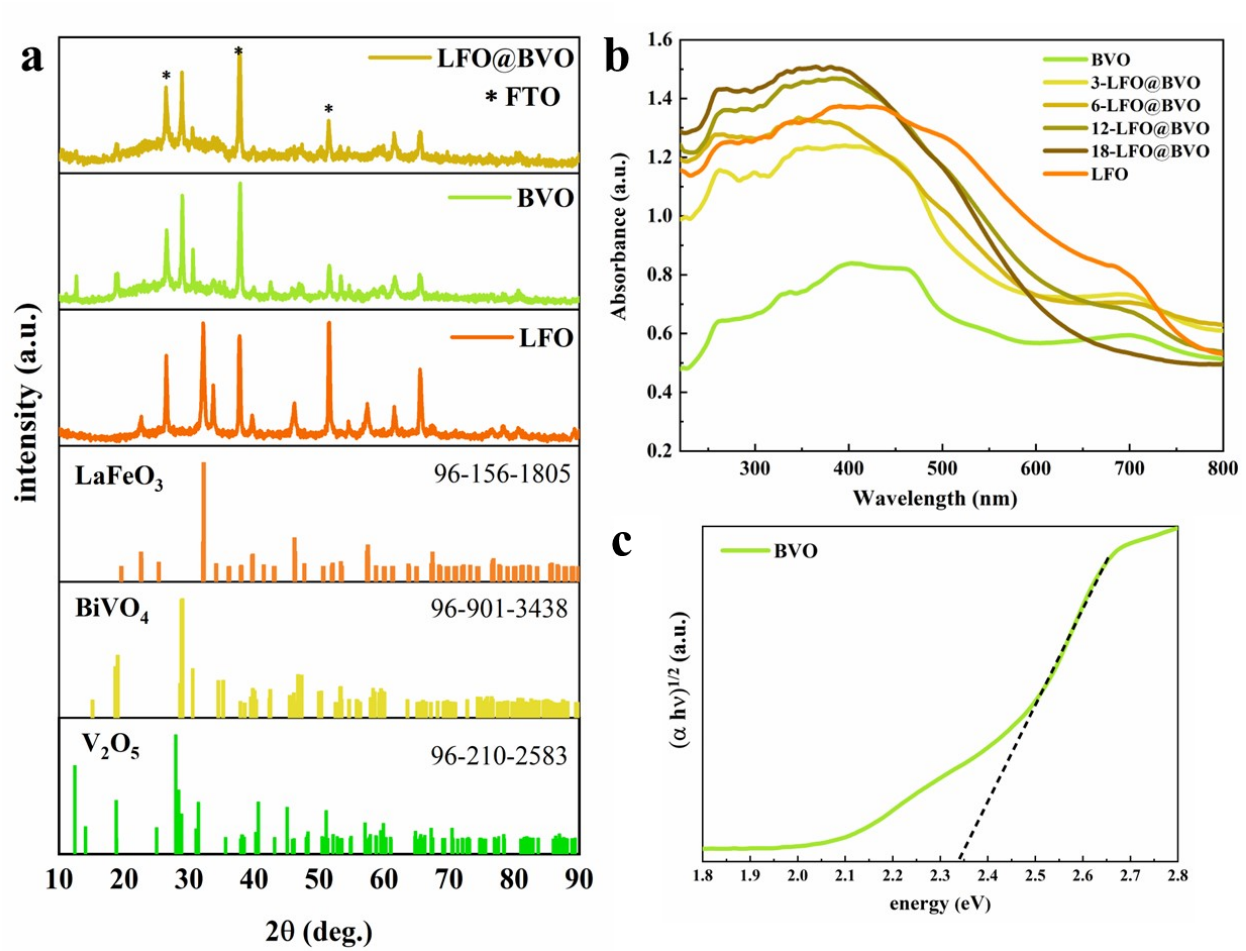

Fig. S3 XRD patterns of LFO, BVO and 12-LFO@FTO (a), DRS spectrum of all samples (b), Tauc plot of BVO (c).

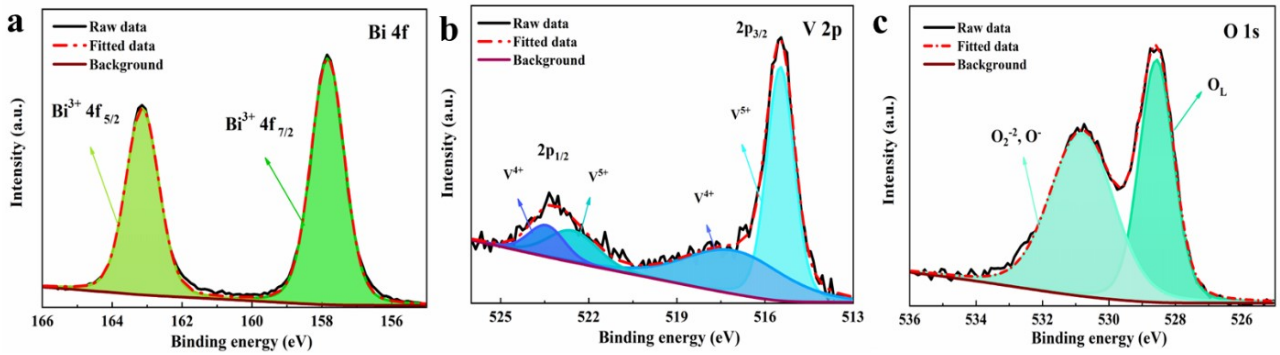

Fig. S4 HR-XPS data of BVO electrode

2. Three-electrode setup

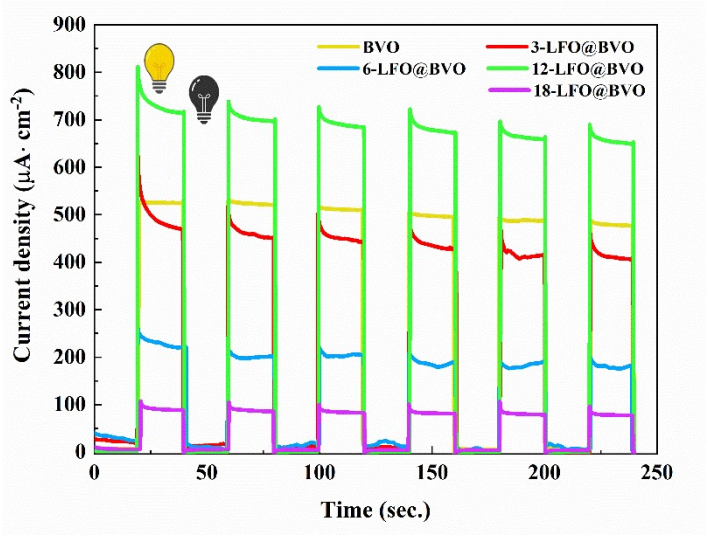

Fig. S5 Chronoamperometry (i-t) plot of all samples under chopped light (20s dark/20s light), at 1 V vs Ag/AgCl (3M KCl) at scanning rate of 5 mV/s.

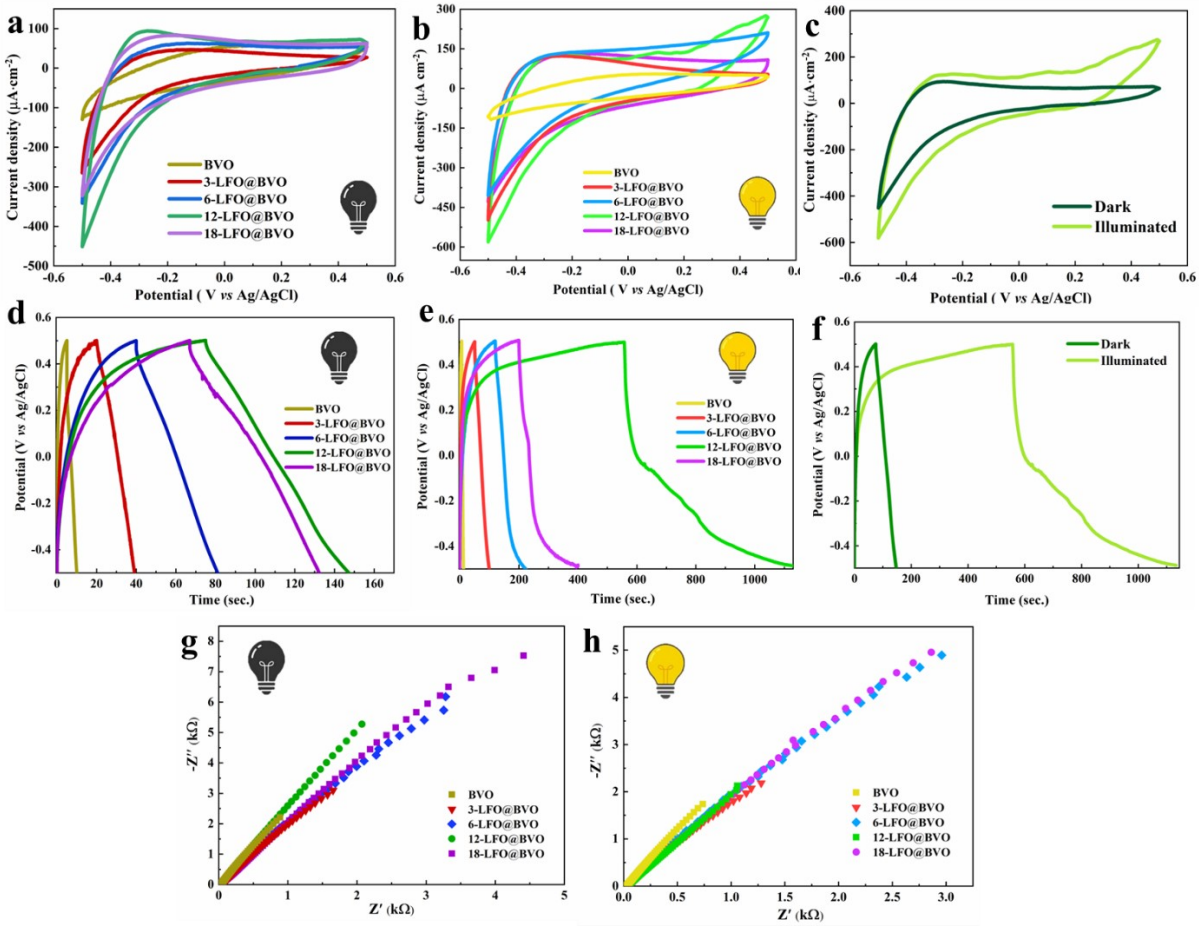

Fig. S6 CV curves of all samples at 5 mV/s in the dark (a) and under illumination (b), CV curves of 12-LFO@BVO (c), GCD profiles of all samples at 0.2 mA cm^{-2} in the dark (d) and under illumination (e), GCD curves of 12-LFO@BVO, Nyquist plots of all samples in the dark (g) and under illumination (h).

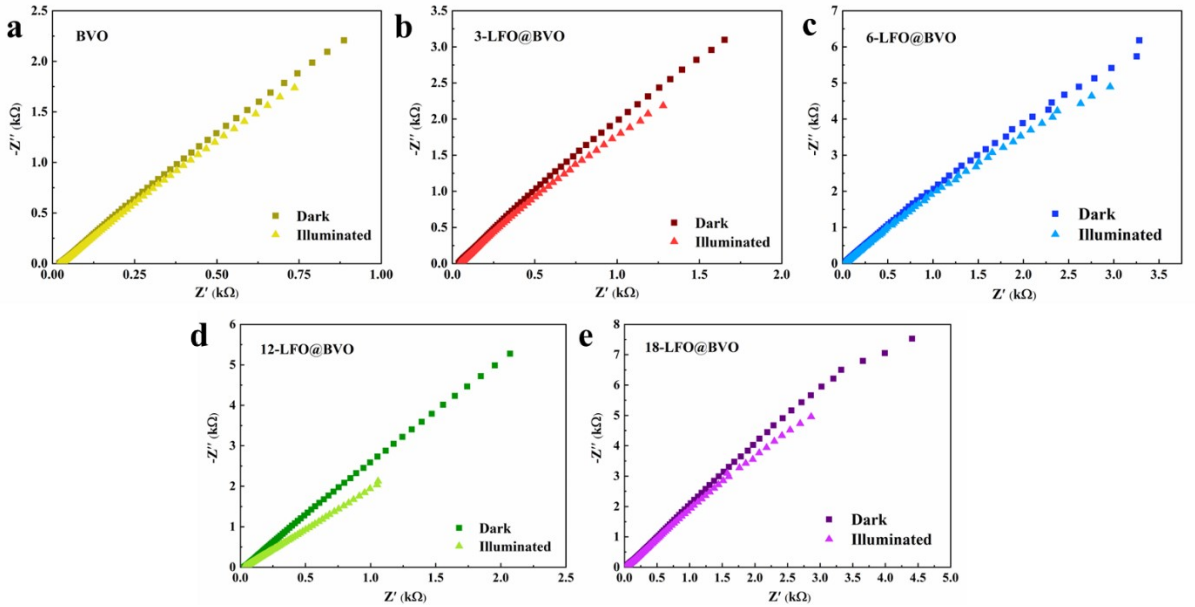

Fig. S7 Nyquist plots of BVO (a), 3-LFO@BVO (b), 6-LFO@BVO (c), 12-LFO@BVO (d) and 18-LFO@BVO (e), in the dark and under illumination.

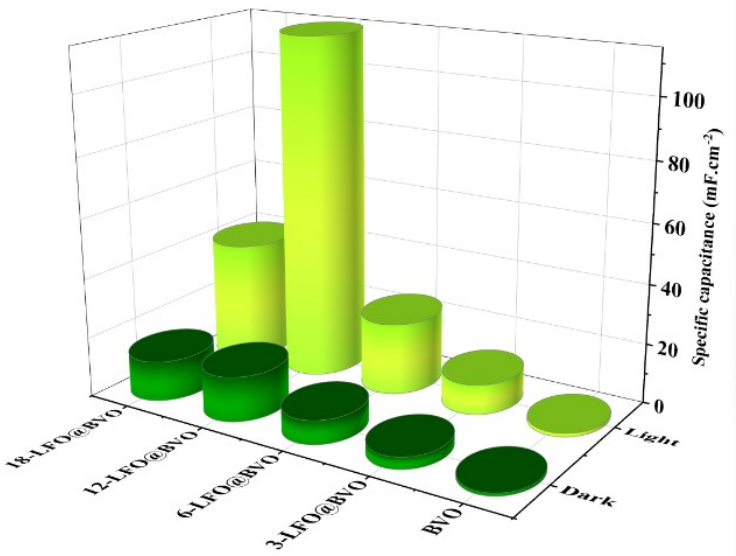

Fig. S8 specific capacitance of all samples in both dark and light conditions. Sample 12-LFO@BVO showed 7.7-fold boost of capacitance upon illumination.

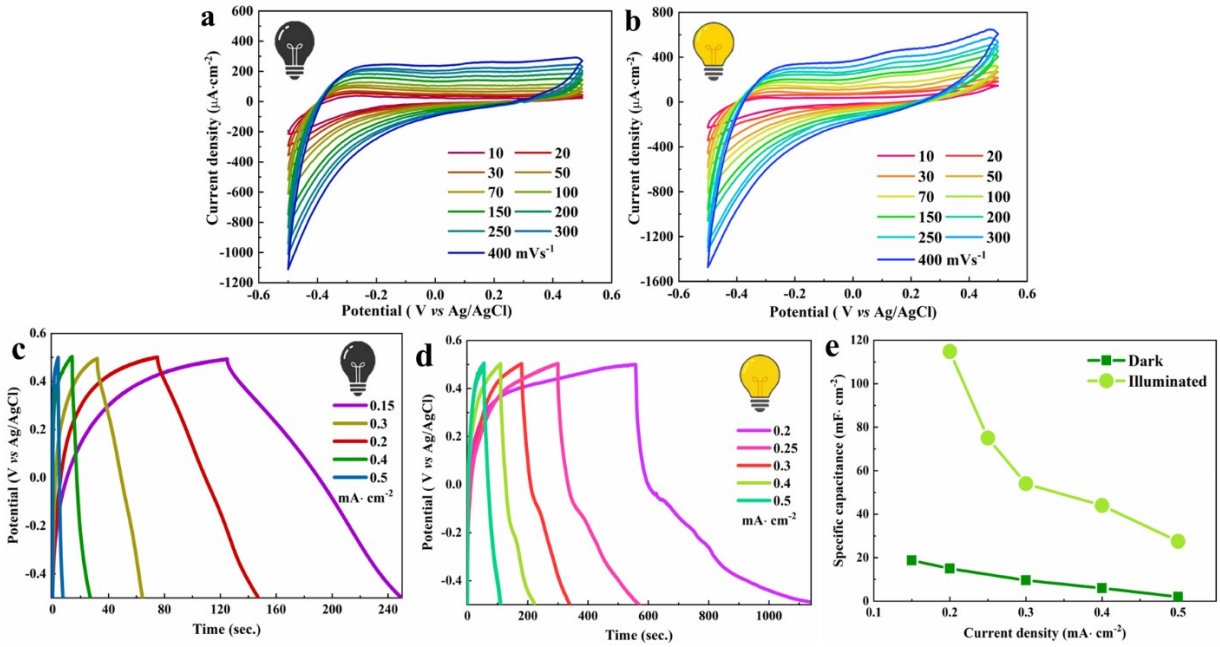

Fig. S9 CV curves at varied scan rates in the dark (a) and under illumination (b), GCD curves at varied current densities in the dark (c) and under illumination (d), rate capability plot (C-i) (e) of 12-LFO@BVO.

Table 1 Comparison of Photocapacitive Enhancement in $BiVO_4$-Based Systems Reported in the Literature and This Work

System / work	Property compared	Approx. enhancement factor under light
$BiVO_4$–RGO bilayer photocapacitor (planar, Na_2SO_4) [1]	Specific capacitance at 0.2 A g^{-1}	Roughly 1.3–1.4× increase (~30–40% higher)
$BiVO_4$–V_2O_5@TiNT based photo-supercapacitor [2]	Areal capacitance at 0.1 mA cm^{-2}	Roughly ~2.7× higher capacitance
Heterostructured $BiVO_4$–PbO photocapacitor ("solar energy storage by $BiVO_4$") [3]	Areal capacitance at ~0.015 mA cm^{-2}	~1.3× increase (≈30% higher)
rGH/$BiVO_4$ aqueous Zn-ion photorechargeable capacitor [4]	Specific capacitance at 0.1 A g^{-1}	1.26× increase (26.3% higher)
Mo:Co coated $BiVO_4$ photoelectrodes for photosupercapacitors [5]	Areal capacitance at 0.02 mA cm^{-2}	50–275 % improvement
General $BiVO_4$-based photochargeable integrated devices (reviewed) [6]	Capacitance or stored charge	Typically, 20–100% higher under illumination
This work	Areal capacitance at 0.2 mA cm^{-2}	~ 7.7× improvement

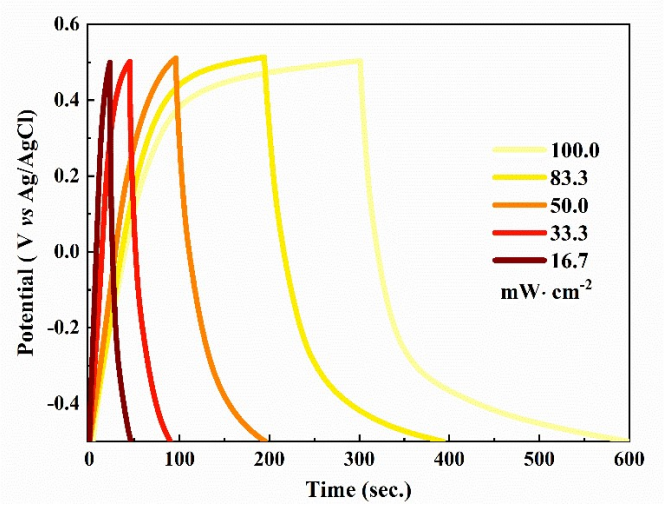

Fig. S10 GCDs of 12-LFO@BVO at 0.5 mA cm^{-2} at under illumination at different light intensities. It shows longer charge/discharge durations as light intensity increases, demonstrating higher stored charge and enhanced capacitance under stronger illumination due to increased photocarrier generation.

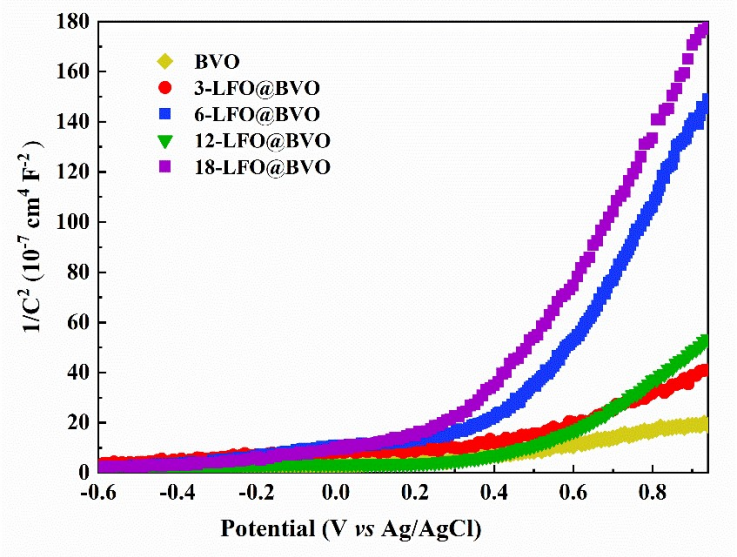

Fig. S11 Mott-Schottky plots of all prepared photoelectrodes

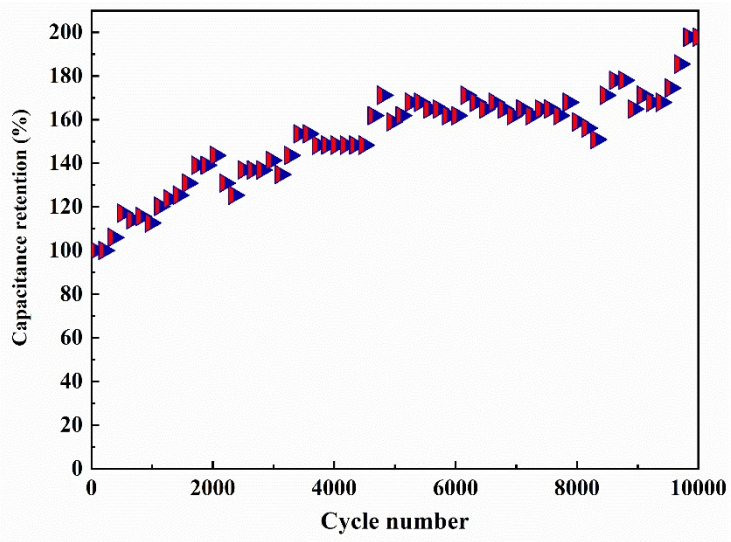

Fig. S12 Cycling stability of 12-LFO@BVO after 10,000 cycles at 0.2 mA cm^{-2}

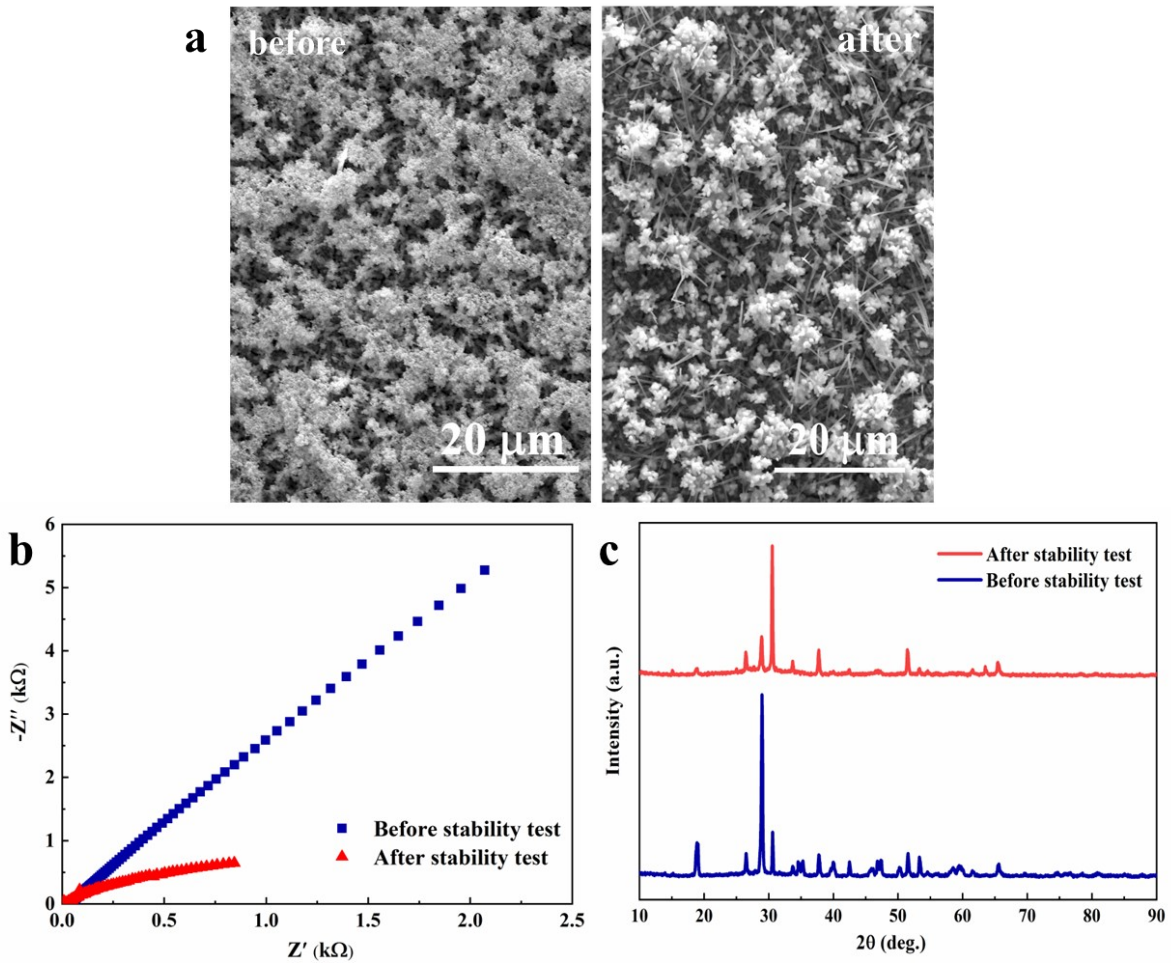

Fig. S13 Evidence of cycling-induced self-activation. (a) SEM images showing the transition from a dense agglomerated overlayer in the pristine sample to an exposed, porous nanoneedle network after 10,000 cycles. (b) Nyquist plots illustrating significant reductions in charge-transfer resistance and diffusion impedance, consistent with the increased active surface area. (c) XRD patterns confirming structural stability with a preferential reorientation toward the active (040) facet.

3. Photo-supercapacitors

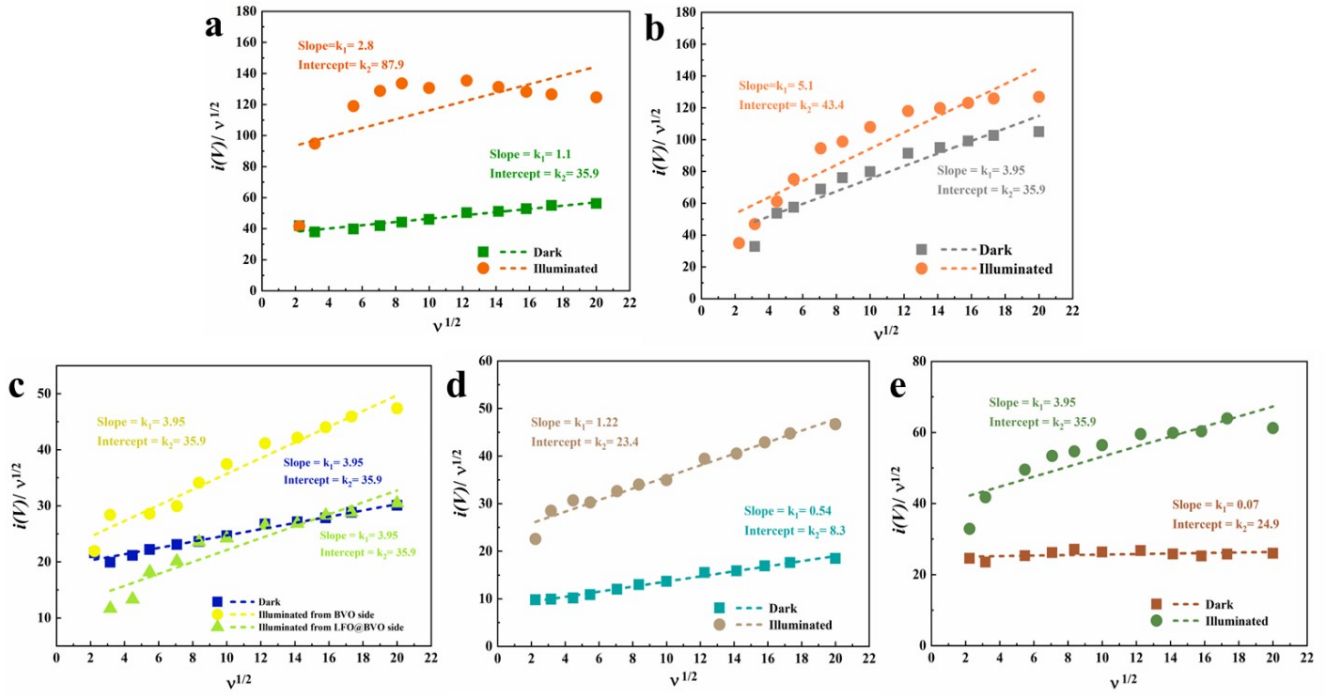

Fig. S14 Plots of $i(V)/\nu^{1/2}$ versus $\nu^{1/2}$ for symmetric LFO@BVO (a), graphite//LFO@BVO (b), BVO//LFO@BVO (c), LFO//LFO@BVO (d), and LFO//BVO (e) PSCs.

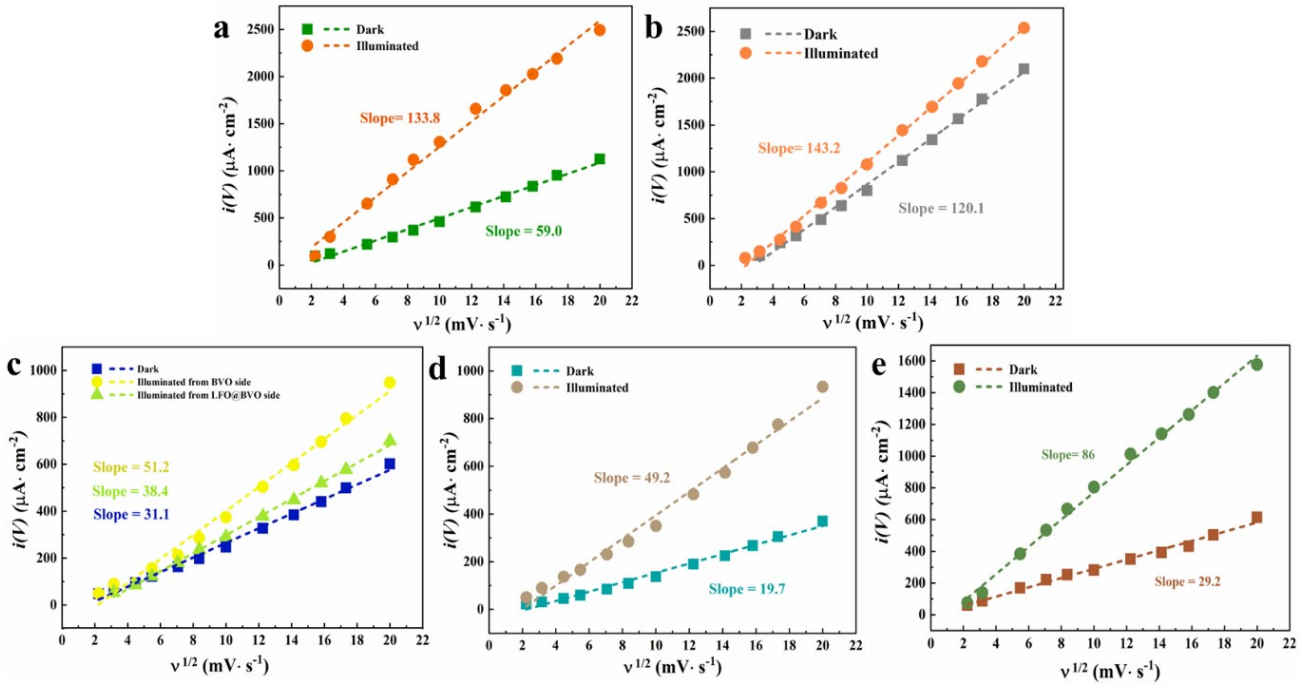

Fig. S15 Comparison of diffusion coefficients in the dark and under illumination for symmetric LFO@BVO (a), graphite//LFO@BVO (b), BVO//LFO@BVO (c), LFO//LFO@BVO (d), and LFO//BVO (e) photo-supercapacitors.

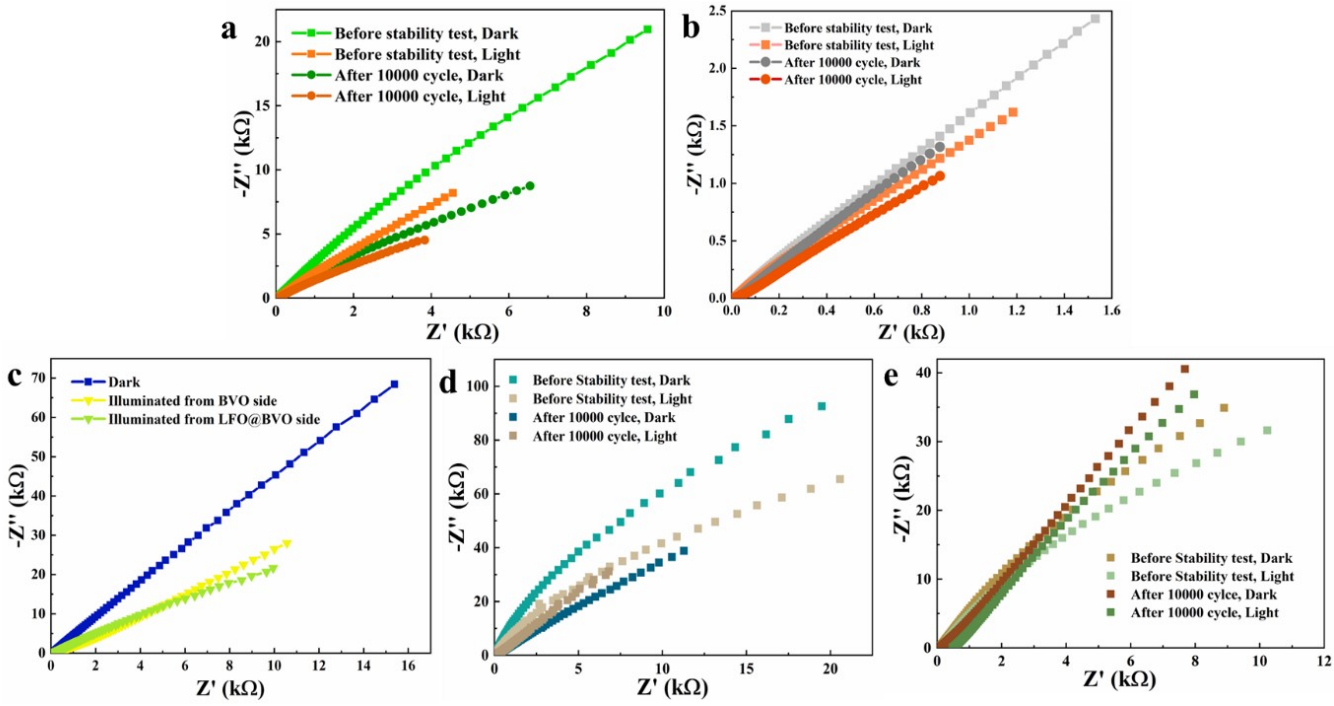

Fig. S16 Nyquist plots of symmetric LFO@BVO (a), Graphite//LFO@BVO (b), BVO//LFO@BVO (c), LFO//LFO@BVO (d) and LFO//BVO (e) PSCs measured at different conditions.

Experimental section

Preparation of BVO photoelectrode

Co-electrodeposition of $BiVO_4$ and V_2O_5 was conducted with a slight modification from previous reports in literature. In short, 10 mM $Bi(NO_3)_3.5H_2O$ (98%, EXIR) was dissolved in a solution containing 35 mM $VOSO_4$ (97%, Sigma-Aldrich). Then 2 M sodium acetate anhydrous (≥99.0%, Titrachem) was added and the pH of the solution was adjusted to 3.7 by HNO_3 (≥69%, Honeywell). A three-electrode system was used, implementing platinum foil, Ag/AgCl (3M KCl) and FTO glass as counter, reference and working electrode respectively. Deposition of Bi-V-O film was carried out at constant potential of 1.9 V vs. Ag/AgCl for 30 minutes, at raised temperature of 70 C. The as-prepared sample was rinsed and annealed at 500 ℃ for 1h (with a ramping rate of 2 ℃/min) to obtain crystalline $BiVO_4$ -V_2O_5 film.

Preparation of LFO@BVO photoelectrodes

Lanthanum ferrite perovskite ($LaFeO_3$, LFO) was electrodeposited on $BiVO_4$-V_2O_5 (BVO) film via a facile electrodeposition using the three-electrode system mentioned above in an electrolyte containing 21 mM $La(NO_3)_3 \cdot 6H_2O$ (99.999%, Sigma-Aldrich), 18 mM $FeCl_2 \cdot 4H_2O$

(99.0%, Merck), and 400 mM KNO_3 (99.0%, Merck). The electrodeposition was executed potentiostatically at -1.09 V, at ambient temperature for variant durations of 30, 60, 120 and 180 seconds. Freshly synthesized samples were rinsed and annealed at 400 ℃ for 2h (with a ramping rate of 2 ℃/min). These samples were denoted as 3-LFO@BVO, 6-LFO@BVO, 12-LFO@BVO and 18-LFO@BVO, respectively.

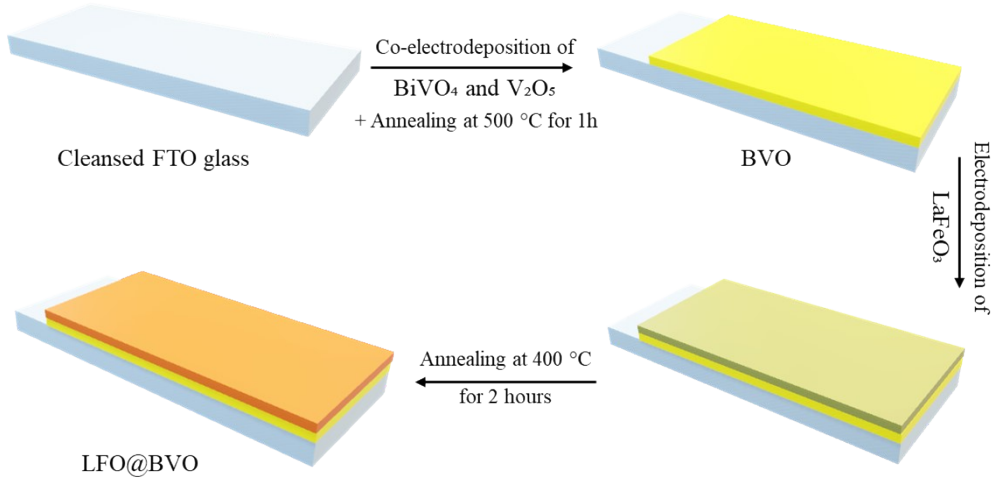

Fig. S17 Schematic illustrating the preparation of the LFO@BVO electrodes

References:

1 A. Roy, P. Majumdar, P. Sengupta, S. Kundu, S. Shinde, A. Jha, K. Pramanik, H. Saha, *Electrochimica Acta* **2020**, *329*, 135170.

2 A. S. Renani, M. M. Momeni, H. M. Aydisheh, B.-K. Lee, *Journal of Energy Storage* **2023**, *62*, 106866.

3 S. Safshekan, I. Herraiz-Cardona, D. Cardenas-Morcoso, R. Ojani, M. Haro, S. Gimenez, ACS Energy Letters 2017, 2, 469-475.

4 C.-b. Zheng, Z.-c. Du, J.-k. Li, H.-d. Jiang, X. Liu, P.-c. Guo, H. Zhu, Y.-x. Wang, *Journal of Energy Storage* **2024**, *92*, 112204.

5 A. S. Renani, Z. Hosseini, D. Eberhart, A. W. Maijenburg, M. M. Momeni, Journal of Power Sources 2025, 640, 236687.

6 C. Tuc Altaf, A. M. Rostas, A. Popa, D. Toloman, M. Stefan, N. Demirci Sankir, M. Sankir, ACS Omega 2023, 8, 47393-47411.